Published in final edited form as:
Magn Reson Med. 2007 July ; 58(1): 156–166. doi:10.1002/mrm.21205.

Development of a Hybrid EPR/NMR Coimaging System

Alexandre Samouilov, **George L. Caia**, **Eric Kesselring**, **Sergey Petryakov**, **Tomasz Wasowicz**, and **Jay L. Zweier***
[1]Center for Biomedical EPR Spectroscopy and Imaging, Davis Heart and Lung Research Institute, Ohio State University, Columbus, Ohio, USA.

Abstract

Electron paramagnetic resonance imaging (EPRI) is a powerful technique that enables spatial mapping of free radicals or other paramagnetic compounds; however, it does not in itself provide anatomic visualization of the body. Proton magnetic resonance imaging (MRI) is well suited to provide anatomical visualization. A hybrid EPR/NMR coimaging instrument was constructed that utilizes the complementary capabilities of both techniques, superimposing EPR and proton-MR images to provide the distribution of paramagnetic species in the body. A common magnet and field gradient system is utilized along with a dual EPR and proton-NMR resonator assembly, enabling coimaging without the need to move the sample. EPRI is performed at ~1.2 GHz/~40 mT and proton MRI is performed at 16.18 MHz/~380 mT; hence the method is suitable for whole-body coimaging of living mice. The gradient system used is calibrated and controlled in such a manner that the spatial geometry of the two acquired images is matched, enabling their superposition without additional postprocessing or marker registration. The performance of the system was tested in a series of phantoms and in vivo applications by mapping the location of a paramagnetic probe in the gastrointestinal (GI) tract of mice. This hybrid EPR/NMR coimaging instrument enables imaging of paramagnetic molecules along with their anatomic localization in the body.

Keywords

proton MRI; EPR imaging; free radicals, oxygen; image coregistration; in vivo NMR; in vivo EPR

The techniques of electron paramagnetic resonance (EPR) spectroscopy and imaging (EPRI) have been widely used to measure and map the distribution of paramagnetic materials and free radicals in biological systems, including ex vivo tissues and in vivo living animals (1–8). These techniques provide unique information that enables measurement and imaging of the processes of free radical metabolism, tissue oxygenation, and nitric oxide generation in normal physiology and disease (9–17). While EPRI provides specific mapping of the location of a given paramagnetic species, this is often not sufficient in itself to enable anatomic mapping of the precise organ-specific location of the paramagnetic probe in the body of a living animal. On the other hand, proton magnetic resonance imaging (MRI) has been established as a powerful diagnostic imaging technique capable of obtaining high-resolution images of the anatomical structure of humans and animals (18–22). While proton MRI is a powerful technique for imaging biological systems based on their high content of water, it can not directly localize low, submillimolar levels of free radicals.

*Correspondence to: Jay L. Zweier, M.D., Davis Heart and Lung Research Institute, Ohio State University, 473 West 12th Ave., Room 110G, OH 43210. jay.zweier@osumc.edu.
Alexandre Samouilov and George L. Caia contributed equally to this manuscript.

Several noninvasive MRI-based methods for detection and mapping of paramagnetic substances in vivo are under development. Both contrast-enhanced MRI (15,16) and proton electron double resonance imaging (PEDRI) (23,24) utilize proton MRI-based detection and therefore automatically provide coregistration of free radical distribution with anatomical structure. The availability of anatomic information, as well as superior spatial and temporal resolution, make MRI-based techniques more efficient in these aspects compared to direct EPRI methods. However, since these techniques are based on spin exchange relaxation or saturation transfer from electron spins to water protons, they are inherently indirect. Furthermore, their application is limited to water-soluble paramagnetic substances, and typically high concentrations (>1 mM) are required for optimal image contrast or enhancement. The application of lipophilic or solid-state paramagnetic probes is problematic. While PEDRI is best suited for measurements of radicals with long relaxation times and sharp linewidths, EPRI has been shown to be much more versatile, enabling imaging of a broad range of soluble and particulate probes with EPR linewidths from 0.002 to 1 mT. The NMR-based methods lack this versatility.

In view of the importance of free radicals and other paramagnetic species in normal metabolism and disease, and the growing popularity of a broad range of soluble and solid-state EPR probes, there is a great need for techniques that are capable of noninvasively imaging their localization in the body. Since EPR and proton NMR provide complementary image information, and both are based on MR principles with requirements for a static magnetic field and field gradient system, the potential exists to build a hybrid instrument that combines advantages of both methods and correlates free radical distribution with the anatomical structure of the body.

While the concept of building a hybrid system with common magnet and field gradients for EPR/NMR coimaging is straightforward, a number of technical challenges have prevented its realization. These include the need for different magnetic fields and frequencies for each modality, as well as different modes and time domains of gradient operation. Therefore, prior EPR/NMR coimaging studies have been performed using two independent systems: continuous wave (CW)-EPR and higher-field pulsed proton MRI systems. In our earlier study that first reported EPR/NMR coimaging (25), we performed EPRI on mice at 750 MHz (≈0.027T) with proton MRI at 16.18 MHz (0.38T). The images were then computationally scaled, registered, and superimposed using a series of EPR- and NMR-detectable markers. Subsequently, Matsumoto et al. (26) reported coimaging of mice with EPRI at 300 MHz (0.0108T) and proton MRI at 8.5 MHz (0.2T) using a composite resonator assembly in which the sample was moved between the two different magnet systems by means of a sliding mechanism.

Typically, proton MRI and EPRI systems utilize very different magnetic field strengths. For proton MRI, it is generally desirable to work at high field strengths (>0.2T). This is based on the desire for maximum sensitivity as well as enhanced spectral resolution when spectroscopy information is desired. For in vivo EPRI, much lower magnetic fields of 0.01–0.04T are typically used because of the constraints placed by problems with microwave penetration and heating at the higher frequencies required for higher-field operations (27). We previously observed that a frequency of about 800–1200 MHz (field ≈ 27–40 mT) provides good, seemingly optimum sensitivity for samples such as mice (up to 30 mm in diameter) (28), in agreement with earlier theoretical predictions (29). We have also observed that at 0.38T (16.18 MHz), good-quality proton MRI images can be obtained with the submillimeter resolution required for EPR free radical image registration (25). Thus, proton MRI at 0.38T has been shown to provide sufficient resolution for anatomic image registration.

Our prior studies demonstrated that proton MRI is an ideal approach to provide anatomic registration of EPR images. While this can be performed using separate EPRI and proton MRI instrumentation, the use of separate instruments requires time-consuming registration of the two coordinate frames, and the movement of the animal from the EPR to the NMR system limits the quality of this image registration and greatly restricts or prevents the performance of many experimental protocols. To achieve accurate and timely image registration for a given experimental protocol, it would be highly beneficial to have dual-mode EPR and NMR imaging capability in one instrument. This hybrid instrument would intrinsically provide high-quality anatomic image registration and enable correlation of the unique information obtainable from EPR- and NMR-based MRI. Based on this need, we developed a unique hybrid EPR/NMR MRI instrument to facilitate in vivo imaging and anatomic localization of free radicals and other paramagnetic species in small living animals.

MATERIALS AND METHODS

Overall System Description

The system utilizes common magnet and gradient coils. The block-diagram configuration is shown in Fig. 1. The MRI acquisition is controlled by an MRRS MR 5000 console (MR Research Systems). This console is equipped with a digital RF system, broadband transmit channel covering 5–1000 MHz for EPR excitation, a broadband NMR transmit channel covering 100 KHz to 300 MHz, and broadband NMR receive channels covering 10 KHz to 300 MHz. The MRRS console is interfaced with an NMR RF amplifier (ENI LPI-10), a two-channel NMR preamplifier (Advance Receiver Research), and two transmit/receive (T/R) switches (Resonex). The main magnet, RF preamplifier, and T/R switches are located inside a double-layer copper-mesh RF shield (Lingren RF Enclosures). The magnetic field gradient system is controlled by three digital signal processor (DSP) waveform generators in pulse mode connected to Copley field gradient power supplies.

The EPRI acquisition is controlled by a PC-compatible computer (Windows XP operating system) that is interfaced with a Bruker ER023 signal channel and Bruker ER032M field controller by an IEEE-488 bus using a GPIB board (Capital Equip, 800EX). The magnetic field gradient power supply control signals, in EPRI mode, are formed by three digital-to-analog (D/A) data acquisition boards (KPC1-3116, Keithley Instruments, Inc., OH) and sent to the Copley gradient power supplies. The L-band microwave bridge is similar to that previously described in Ref. 30 and utilizes a laboratory-built, cavity-stabilized microwave oscillator with maximum power output of 320 mW.

Magnet and Magnet Power Supply

The magnetic field B_0 is generated by a water-cooled iron-core resistive magnet (5000/Paradigm; Resonex Corp.) with a gap of 50 cm with shims in place (Fig. 2). The magnet is equipped with a set of 24 active shim coils that provide homogeneity of better than 50 ppm over a clinical whole-body sample size of 50 × 40 × 40 cm, and better than 20 ppm over a 25 × 20 × 20 cm sample volume. Its magnetic field is vertically oriented, but otherwise it is similar to the iron-core resistive magnet designs used in conventional EPR spectrometers.

In order to accommodate a new removable gradient coil system, the magnet was modified. To preserve the original whole-human-body capability of the magnet system, rather than simply removing the original clinical Resonex gradient coils, the coils were moved closer to the magnet poles to be even with the surface of the magnet's iron passive shims and expand the overall magnet gap. The new gradient coils used for EPR/NMR coimaging were mounted on a rail mechanism to slide in and out of the magnet, providing ease of interfacing

and setup along with convenient access for service and further modifications of the gradient coils and the magnet. Rails were installed in the magnet gap to support the load of the new gradient coils. The rails were made out of a fiberglass/epoxy composite (grade G-10/FR4 Garolite) in the form of rectangular bars, and could be extended to both ends of the magnet for easy displacement of the gradient coils to clear the magnet gap for other experiments and easy maintenance. Gradient coils experience significant mechanical forces due to the interaction of gradient currents with the main magnetic field. Therefore, to avoid flexing (which may affect the coregistration accuracy), rigid fiber-reinforced epoxy plastic was chosen as a structural material for the gradient coil rolling mechanism. Gradient coil (re)positioning was accurate to 0.5 mm along the Z, Y, or X directions. Once the gradient coil assembly was inserted into the magnet, its position was fixed.

The magnet is powered by a Danfysik power supply (model MPS 854/SYS 8000; Denmark) that can provide current up to 2000 amps required to reach 0.38T. In MRI mode, the magnetic field is current-controlled and its stability relies on the high-precision, manually adjustable reference voltage. This regulation guarantees high stability better than 0.5 ppm/hr of the current and hence magnetic field. To add the capability of a computer-controlled field-sweep required in the EPRI mode, the power supply was modified. A switching circuit was added that allows the reference voltage in the Danfysik power supply to be substituted by a voltage generated by the Bruker ER032M field controller. With this provision, the magnetic field can be set manually to any value between 5–400 mT in current-controlled mode or automatically swept under computer control with the Bruker ER032M field controller. The magnetic field can be swept from 5 to 400 mT in less than 10 s. The set of shims supplied with the magnet can be programmed to provide high field homogeneity over the full range of magnetic fields from 5 to 400 mT.

Changing the mode from a low-field EPRI acquisition (typically ~40 mT for L-band operation) to proton MRI (typically 380 mT) takes less than 5 min, although an additional 10 min is required for MRI field stabilization. The reverse change from MRI to EPRI mode can be executed in less than 2 min.

Field Control and Regulation

As noted above, our system utilizes a large iron-core electromagnet that enables a quick transition from low-field EPR measurements to proton MRI measurements at much higher fields. Since iron-core electromagnets exhibit hysteresis, a repetitive sweep of the electrical current, as required for EPR data acquisition, does not result in a precisely reproducible magnetic field sweep. Therefore, as is the case in commercial EPR systems with iron-core magnets, closed-loop regulation of the magnetic field in the form of a Hall probe field sensor and corresponding field controller was utilized for EPR data acquisition. For proton NMR and MRI, however, a precise, stable, fixed magnetic field is required, and this was best accomplished with current control. For transition from EPRI to proton MRI acquisition, the magnet power supply is switched from the field control to the current control mode.

For EPR operation, field control and regulation were achieved with the dual Hall-effect magnetic field probe approach and Bruker ER032M field controller with closed-loop feedback, as we have previously described (31). Whereas in the prior study two specially constructed Hall probes were positioned on the Z-axis (along B_0 field) of the gradient coil system at equal distance from the center of the gap, in the current coimaging system, due to space limitations along Z, the Hall probes were installed along the X-axis (horizontally across the magnet gap; see Fig. 2). The Hall probes are attached to the movable frame that bears the gradient coils. The Hall probe fixtures allow easy adjustment of the probe position in 3D and reliable fastening.

Dual hall probes mounted in thumbscrew-adjustable X, Y, Z fixtures were first roughly positioned at Z- and Y-dimensional midpoints. A readily mechanically accessible X position was also selected. The beginning Z and Y positions of the first probe were set with the second probe out of gradient influence in an iterative process using a 3-Hz triangle modulation to excite the gradient amplifier for the axis under alignment. The command voltage output of the Hall probe field controller was monitored with an oscilloscope as the first Hall probe was moved to a position that produced minimum amplitude. The second probe was then installed and roughly positioned in X, Y, and Z. Fine second probe positioning was continued by adjusting in a Z, Y, X iteration until the field controller output was minimized. The thumbscrews in the hall probe fixtures were then tightened to secure the alignment.

The Hall elements are connected in series and excited by the field controller. Balancing resistors are connected in parallel to the Hall elements to compensate for difference in sensitivity of the individual elements. The outputs of the Hall elements are added and scaled in a matching transformer, so that the field controller reads the average Hall voltage corresponding to the magnetic field B_0 in the center of the observation volume (Fig. 3). The Y-gradient generates shifts of Hall voltage that are equal in magnitude, but with opposite polarity for each probe. Summing of the voltages eliminates the perturbing effect of the Y-gradient. Hall effect elements (model HR-125A) were obtained from Ohio Semitronics. The elements are mounted on noninductive thin-film ceramic substrate resistors, which serve as thermostat heaters. A chip thermoresistor from BC Components attached to the assembly provides feedback to the temperature controller. Tight temperature regulation (±0.025°C) ensures stability of the magnetic field. Hall probes were matched and interfaced to the Bruker ER032M field controller.

The activation of the gradient coils (triangular pulse shape of 2.9 mT/cm at 3 Hz frequency) does not alter the voltage on the input of the main power supply, ensuring that the Hall probe sensor setup is not sensitive to the gradient field.

Gradient Coils and Gradient Power Supplies

The gradient coil set used for both EPRI and proton MRI was provided by Tesla Engineering. It is a set of planar 3D field gradients that is interfaced to the gradient power supply amplifiers. This common gradient set ensures a common image coordinate system with automatic registration of the EPR and proton MR images. The water-cooled 3D gradient coils are planar pairs each of 20 mm thickness with 650 mm diameter and an open gap of 140 mm. The gradient coils have low resistance and low inductance (X and Y coils: 85 μH/50 mΩ; Z coil: 67 μH/30 mΩ) and provide a gradient strength of 1 mT * m^{-1} * A^{-1} with linearity of about 5% in a spherical volume of 80 mm. Gradient coils for the X and Y directions are in distributed current mirrored D design, and Maxwell coils are utilized for Z. The gradient coil set is capable of generating a pulsed gradient (ramp time with existing power supply 125 μs from 0 to 204 mT/m) or sustained gradient of 294 mT/m along the X, Y, and Z axes. The gradients are powered by a modified Copley 235 three-channel switching amplifier capable of 300 A per channel, controlled by the MR5000 MRI console or by our EPRI data acquisition system through Data Translation communication board, model DT-2823, in EPRI mode. Cooling of the gradient coils (maximum power dissipation = 21 kW) is provided by a separate water circuit heat exchanger (model TE20411; Eaton-Williams, Edenbridge, UK) that shares the primary chilled water circuit with the main magnet. Gradient coils are equipped with 16 resistance temperature detectors (RTDs) connected to an external scanner interfaced with a safety interlock system that also monitors cooling water flow and temperature, as well as current in the magnet windings.

Stage for the Dual EPRI/MRI Resonator

Since a goal of the EPR/NMR coimaging system design was to avoid movement of the sample relative to the magnetic field gradient coordinate system, a dual-purpose resonator assembly was developed that contains an EPR and proton NMR resonator with stage that enables each resonator to slide precisely into place around a fixed sample-holder located at the center of the gradient system (Fig. 4). The sample-holder is made out of a polystyrene tube by cutting out half of its circumference over a length of ~70 mm. The sample-holder is rigidly connected to the support tubes on both sides, which are made out of Plexiglas. The outside surface of the Plexiglas tubes is painted with electrically conductive silver paint (DuPont 4922N-50 silver composition acrylic; Delta Technologies Ltd.) for electrical shielding. Tubes are attached to the front and back walls (PVC plastic) of the positioning stage. This architecture was chosen to facilitate in vivo animal experiments, as it allows convenient loading of the animal or sample either through the top of the sample-holder or from the front side of the magnet through the support tubes. The tubes and object-holder have the same inner diameter (ID = 32 mm). Easy access to the sample facilitates monitoring and supporting the physiological state of the animal during the experiment. The two side walls (PVC plastic) of the positioning stage have tongues that precisely fit into matched grooves in the resonator outer housings (Capron plastic) and allow smooth and precise sliding of the resonator housings along the stage. Resonator housings are linked with each other by two platforms that protrude outside the side walls through the slots in the walls. These platforms also support RF feeds, as well as the tuning and coupling controls for both resonators including the semisphere knob (which allows the “remote” adjustment with use of a matched plastic extension rod when the setup is in the magnet gap), gear rotation direction changer, and flexible joints that allow smooth adjustment of the EPR resonator coupling. A locking mechanism (spring-loaded stop plunger) is located in the center of the positioning stage side wall. Corresponding notches are machined in the resonator housings and provide precise positioning of the resonators around the sample for either EPRI or proton MRI. Mechanically, the resonator stage setup allows reproducible repositioning of the resonators with 0.2-mm accuracy along X, Y, and Z.

EPR and NMR Resonators

A 16-gap loop-gap L-band resonator (1.21 GHz, ID = 43 mm, length = 48 mm) was built. The 16-gap design with gaps oriented radially from the center enabled a larger-diameter resonator to be built for this frequency than would be possible with a lower number of similar gaps, and provided good homogeneity of the B_1 magnetic field similar to design concept resonator. This design concept was previously demonstrated to provide good spatial separation of E and B_1 fields (17,32). The dimensions of the resonator were chosen to accommodate and obtain EPR images of the whole body of a living mouse, which requires at least a ~ 30-mm diameter. Since this resonator was designed with an EPR/NMR coimaging setup, the ID of the resonator had to be increased to 42 mm to accommodate our specialized coimaging sample-holder. An additional advantage of this multigap design is that field modulation penetrates more effectively between the multiple gaps. All elements are enclosed in a nylon housing that provides mechanical rigidity, and this housing is silverplated to serve as an RF shield. The resonator is magnetically coupled. The quality factor Q of the empty resonator measured using a RF network analyzer was 240, and it dropped to 120 with a resonant frequency of 1.16 GHz when loaded with a 25-g mouse. The efficiency of the empty resonator measured by the method of perturbing spheres according to Ref. 33 was 0.25 mT $W^{-1/2}$.

Modulation coils of square shape (45 turns of litz wire with 49 strands of 0.07 mm) with dimension 88 × 88 mm are connected in parallel. The sum inductance is 108 μH, and the resistance is 1.3 Ω at DC and 68 Ω at 100 kHz. The modulation coils are positioned between

the resonator and the shield to provide >90% homogeneity over a cylindrical volume of 44-mm diameter and 44-mm length, and achieved a modulation amplitude of up to 0.15 mT at 1.9 W power dissipation. Modulation coils are powered through a Haffler FG-P3000D amplifier in non-resonance mode, typically at 100 kHz.

A conventional solenoidal coil NMR resonator made of 6.5 turns of silver-plated copper foil (12 mm wide, 0.25 mm thick) turned around and glued to a fused quartz tube (outer diameter (OD) = 45 mm, ID = 42 mm) was used. The ID of the resonator was 42 mm with a length of 100 mm. The resonant frequency of the loaded resonator was 16.18 MHz, and *Q* measured on a RF network analyzer was 120. The equivalent inductance was 3.2 μH. An external tuning/coupling capacitance (9–50 pF/0–50 pF) box was used.

Software for Data Acquisition and Image Analysis

The MRI data acquisition is controlled by MR Research Systems MRRS NMR Launcher version 6.2 software running on a Pentium computer with a Windows NT operating system. The software includes a digital signal processor, pulse programmer, RF waveform generator, and oblique gradient waveform controller. A programming environment is provided with pulse programming capability, waveform editor, image reconstruction, and display modules. Our in-house-developed software package (EPR2000) was used for EPRI acquisition, field sweep control, and image reconstruction.

A PC with a 3.2-GHz processor and 1 GB of RAM with the Windows XP operating system was used for detailed image analysis. The raw MRI data were imported and reconstructed using software written in Matlab 7 (MathWorks, Natick, MA, USA). The MRI raw data were reconstructed from the *k*-space data using Fourier reconstruction in 3D. The EPRI data were imported after they were reconstructed in the EPR2000 software. A Matlab-based program was developed to allow slicing, rotating of the 3D image results, postacquisition filtering, contrasting, and merging of the proton MR image data with the complementary EPR image data. After the 3D datasets were reconstructed and sliced for quantitative analysis and presentation purposes, they were fused in 3D and/or slice by slice in 2D using distinct color schemes for the MRI and EPRI modalities.

Phantom Manufacturing

A phantom consisting of four rectangular hollow bars made from optical plastic cuvettes filled with 1 mM of 2,2,6,6-tetramethyl-4-oxo-piperidine-N-oxyl (TEMPONE) (Fig. 5a) and glued together was used for calibration of the gradients.

A phantom with a more complex structure (Fig. 6a) was built to test the resolution of the system. The outer layer was machined out of a polymer tube (OD = 32 mm) that fit snuggly inside the resonator sample-holder. Five grooves were milled out on the outer surface along the longitudinal axis of the tube to accommodate five glass capillary tubes (cut from 100-μL glass pipettes, ID = 1.1 mm). Four of the tubes had a length of 50 mm, while the fifth one had a length of 10 mm. The fifth short tube was inserted in an asymmetric way to provide a means of indexing the coronal plane direction. Inside this assembly a 20-mm-long cluster of 70 capillary glass tubes (cut out of 50-μL glass pipettes, ID = 0.5 mm) was inserted, bound together into a triangular prism shape. The 1.1-mm and 0.5-mm tubes were filled with a 1-mM solution of Tris (8-carboxyl-2,2,6,6-tetramethylbenzo-[1,2-d; 4,5-d′] bis [1,3] dithiol-4-yl) methyl sodium salt (TAM) (34,35). The EPR spectrum of this radical is a single line with a linewidth of ~0.024 mT under aerobic conditions. Along the three sides of the triangular cluster of capillaries were inserted three larger tubes (ID = 9 mm, length = 50 mm) filled with distilled water. Since the larger tubes (ID = 9 mm) are filled with water, they should be

visible only in the proton MRI image. The medium tubes and the thinnest should be visible in both imaging modes since they are filled with aqueous TAM solution.

In Vivo Animal Studies

Female C3H mice of about 25 g weight were obtained from Charles River Laboratories (Wilmington, MA, USA). In preparation for the experiments the mice were fed for approximately 12 hr with mouse food (Teklad LM-485; Harlan, Madison, WI, USA) mixed with the charcoal EPR probe (activated carbon, Darco® KB-B, −100) in 1:1 proportion by volume. All measurements were performed under ketamine/xylazine anesthesia (200 mg/kg and 4 mg/kg, respectively, i.p.). The anesthesia was maintained for a period of ~1 hr—enough to acquire a series of EPRI and proton MRI images. The anesthetized mice were placed inside a polymer tube (OD = 32 mm, ID = 28 mm) open at both ends.

RESULTS

Phantom Studies

EPR and proton MRI images of test phantoms were obtained to check the alignment of the resonators and the calibration of the magnetic field gradients. The simple symmetric rectangular structure of the plastic cuvette phantom aligned with the gradient axes facilitated independent calibration of individual gradients in both EPRI and proton MRI modes. Since the phantom was precisely positioned along the axes of the gradient system, this allowed the use of 2D acquisitions for EPRI gradient calibration. Gradient strengths for both EPRI and proton MRI modes were calibrated in such a way that at a predetermined field of view (FOV), the dimensions in all directions coincided with the actual dimensions of the phantom. Fusing of the resultant images showed a good match between EPRI and proton MRI (Fig. 5b). This phantom had relatively large homogeneous regions and enabled assessment of the homogeneity of the B_1 component of the RF fields of each resonator (36). Uniform 2D image slices were obtained for both EPR and proton MR experiments, indicating that good B_1 homogeneity was achieved for both resonators.

Slices from the 3D EPR and proton MR images contained well-resolved details of another capillary tube phantom. In Fig. 6b, side-by-side proton MRI and EPRI slices, as well as fused images, are shown in axial view. As above, a grayscale is used for presentation of the MRI data, and a hot-metal color scale is used for the EPRI data. In Fig. 6c views of the renderings of the full 3D datasets are shown side by side, along with a view of the fused 3D images. From these images we see that the achievable resolution is better than 0.6 mm for a 50 × 50 × 128 mm FOV, which is required for whole-body mouse images. Fusing of the images shows that any misregistration between the EPR and proton MR images is very small and maximal at the edges of the images, where it is one pixel or less of the acquired image resolution, or less than 0.4 mm.

Studies in Living Mice

Additional studies were performed to assess the ability of the EPR/NMR coimaging system to perform 3D EPRI of a paramagnetic probe with proton MRI-based anatomical registration of its distribution within the body of a living mouse. The goal was to obtain 3D image data from a small living animal in a reasonably short time suitable for physiological studies. To limit time-dependent changes of the image, a stable paramagnetic charcoal EPR probe was used that was previously shown to be useful for EPRI of the gastrointestinal (GI) tract following oral administration. Special care was taken during the experiment to keep the animal anesthetized and immobilized. The charcoal EPRI probe was administered to the animal by mixing it with the standard food. This material is stable in biological systems and

is not absorbed from the GI tract. It has a single-line EPR spectrum with a linewidth of 0.07 mT under aerobic conditions.

The sample-holder tube, with the anesthetized mouse lying on its back inside, was placed horizontally inside the resonator's sample-holder. In Fig. 7a side-by-side views of the 3D MRI image dataset (grayscale), the 3D EPRI dataset (color scale), and the fused view of the images are shown. In Fig. 7c–e the coronal, axial, and sagittal slices are shown, respectively (the slice number is inserted in each figure). This combined imaging experiment was completed in 40 min. The fused images enable visualization of the location of the paramagnetic probe within the abdomen and GI tract of the mouse. The location of the char in the GI tract visualized in the EPR image overlays the voids in intensity associated with the GI tract seen in the proton MR images. Thus, coimaging was performed in a living animal within a time suitable for physiological studies and provided anatomical visualization of the 3D distribution of the paramagnetic probe within the body.

DISCUSSION

While great progress has been made in the development of instrumentation and techniques for EPRI, it has become clear that this technique has certain fundamental limitations that can only be overcome by augmenting EPRI with other complementary imaging modalities. EPRI provides a spatial map of the distribution of free radicals or other paramagnetic species (25); however, it does not typically provide anatomical registration of organ-specific locations within the body. Therefore, it is of critical importance to combine EPRI with a complementary imaging modality that can provide this anatomic localization. Proton MRI is well suited to provide such anatomic imaging data, and has the advantage over other medical imaging techniques in that, as an MR-based technique, it also makes use of a magnetic field and field gradient system. If the same magnet and gradient system are used for both EPRI and protonbased MRI, proton NMR image datasets can be acquired that are intrinsically coregistered with the superimposed coordinate frame obtained by EPR-based imaging.

In the present work, we have described the development of a hybrid imaging spectrometer system that enables both EPR and proton NMR imaging within the same magnet and gradient system. The common magnet eliminates the need to transfer the sample, minimizing the transition time from EPRI to proton MRI measurements. The common gradient coils remove the need for computational postprocessing and alignment of markers to achieve coregistration of these EPR and NMR images. Also, with this design, the superposition accuracy of the EPR/NMR images coregistration does not rely on the mechanical tolerances of the resonators, gradient coil assembly, or their positioning in the magnet; rather, it relies on the accuracy of the gradient power amplifier calibration for EPR and NMR experiments. The results of the phantom experiments demonstrated a 0.4-mm overall superposition accuracy. The system has the major practical advantage that the visualized object is immobilized in both working modes of the system and remains in the same position. This prevents the possible displacement of the object from a given set of markers or changes that could occur based on its movement or repositioning from system to system. Overall, this instrument enables the rapid acquisition of EPR image data along with proton MR images that can be used for anatomic image registration.

Four main components of our system make it conceptually novel in comparison to previous approaches for EPR/ NMR coimaging (He, 2002 #45) (26). First, the iron-core resistive magnet has the ability to freely and rapidly sweep the magnetic field from 0T to 0.38T. This is a big advantage over permanent magnets or superconducting magnets that are either fixed in field or only slowly adjustable with loss of cryogens, respectively. The resistive magnet design allows for easy variation of the magnetic field from the higher fields that are

desirable to enhance NMR sensitivity to the lower fields required for in vivo EPRI. The magnetic field range used for proton MRI was 0.38T near the maximum capability of the magnet system, while that used for EPRI was constrained by the microwave penetration of the tissue; hence 40 mT (~1.1 GHz frequency) was chosen for imaging of living mice. The second critical feature is the use of the same gradient coils in both EPRI and MRI modes. The control of the gradient coils is performed in continuous mode for EPRI and in pulsed mode for proton MRI.

A third feature is that the magnetic field is controlled in either current control mode for the maximum fixed field stability required for NMR, or with Hall probe-based field regulation as needed to reproducibly sweep the magnetic field of the resistive iron-core magnet for EPR acquisition. Hall probe-based field regulation eliminates hysteresis-based field shifts. A novel double Hall probe approach was implemented to prevent gradient-mediated pulling of the magnetic field. For EPR field regulation, the Hall probe is usually placed on one of the magnet pole pieces; however, in the presence of field gradients, a single Hall probe is not sufficient since the gradient coils produce “pulling” fields and thus the correct static field will not be maintained. In the double-Hall-probe scheme implemented in our system, Hall probes are placed at equal distance along the Y-axis, at the null in X and Z, so that the magnetic field gradient along Y generates shifts of Hall voltage on both probes that are equal in magnitude but have opposite polarity for each probe, while gradients along X and Z have no effect. After the voltages are summed, the perturbing effect of the Y-gradient is eliminated.

The fourth feature, the dual resonator assembly, has an innovative design in which two different resonators (one for EPR and the other for NMR) slide along the positioned and immobilized object. Coaxial design of a dual-purpose resonator in principle is possible (26); however, mutual interference, which can degrade the resonator’s performance, and the possibility of interference of the EPR resonator shield with proton MRI gradient pulses were a concern. Since EPRI and MRI are performed at different B_0 values and at different times, we used separate EPRI and MRI resonators placed on a precision positioning stage. This approach is more flexible, since this positioning stage can be equipped with any desired resonator so that EPR and NMR spectroscopy and imaging can be supported at any desired frequency or sample size. The main requirements for the design of the positioning stage were to precisely and reproducibly position the EPR and NMR resonators in place around the sample, and to be able to conveniently adjust their tuning and coupling.

The performance of the hybrid EPR/NMR coimaging system was evaluated in a series of phantoms and in living mice. Since CW-EPRI, unlike pulsed proton MRI, is not slice-selective, to acquire quantitative 3D information about the spatial distribution of the paramagnetic species a full 3D acquisition of the whole FOV that includes the object must be performed. This can then be correlated with the high-resolution 3D proton MRI image of the same object. The acquired datasets can then be fused and analyzed slice by slice in 2D or examined in 3D views. Imaging of a series of phantoms of simple or complex geometry clearly demonstrated that the EPR/NMR coimaging instrument provided intrinsically registered images that were superimposable along all three dimensions to the limit of the acquired image resolution (>0.4 mm). In vivo studies in mice fed a paramagnetic charcoal imaging probe enabled visualization of the location of the probe within the GI tract of the mouse and its anatomic registration within the whole body. It was demonstrated that 3D spatial mapping of the paramagnetic probe was possible with submillimeter resolution. The experiments performed represent the first example of 3D EPR/NMR coimaging in a living animal, and demonstrate the feasibility of performing this type of coimaging in an efficient way suitable for studying the role of paramagnetic molecules in normal physiology and disease. The described hybrid EPR/NMR coimaging instrument greatly facilitates the

efficient and precise mapping of the spatial location of free radicals and other paramagnetic molecules in living mice.

SUMMARY AND CONCLUSIONS

We have developed a hybrid EPR/NMR coimaging instrument that uses the unique capability of EPRI to detect the distribution of paramagnetic materials within biological systems, in combination with the power of proton NMR-based MRI to provide high-resolution mapping of the overall anatomical structure of the body. Our approach has an advantage over past approaches in that the sample is not moved between two different systems. It utilizes the same set of field gradients for both EPRI and MRI that are controlled in either continuous mode for EPRI or pulsed mode for proton MRI, in the same resistive magnet system that can be set to the magnetic field required for either mode. The design of the resonator assembly holds the sample in place and allows either resonator to slide over the sample, eliminating the requirement for spatial markers and image postprocessing to achieve coregistration. Our studies of various samples with different structures show that with calibration of the gradients, and the choice of an identical FOV for both modes, accurately aligned images can be obtained. This instrumentation enables in vivo 3D EPR/NMR coimaging in living animals within a time suitable for physiological investigation. We were able to localize and visualize the spatial distribution of a paramagnetic solid-state material inside living mice and map its location with submillimeter resolution. The whole setup and 3D image acquisition process could be completed within 40 min. Thus, the described hybrid EPR/NMR coimaging instrument greatly facilitates the efficient and precise mapping of the spatial location of free radicals and other paramagnetic molecules in living systems.

Acknowledgments

We thank Dr. Ilirian Dhimitruka and Dr. Frederick Villa-mena for supplying the TAM radical used, Dr. Yuanmu Deng for EPRI software development, and Dr. Periannan Kuppusamy for critical advice.

Grant sponsor: National Institutes of Health; Grant numbers: EB0890; EB4900.

REFERENCES

1. Berliner JL, Fujii H. Magnetic resonance imaging of biological specimens by electron paramagnetic resonance of nitroxide spin labels. Science 1985;227:517–519. [PubMed: 2981437]
2. Eaton SS, Maltempo MM, Stemp EDA, Eaton GR. 3-Dimensional electron-paramagnetic-resonance imaging with one spectral and two spatial dimensions. Chem Physics Lett 1987;142:567–569.
3. Goda F, Liu KJ, Walczak T, O'Hara JA, Jiang J, Swartz HM. In vivo oximetry using EPR and India ink. Magn Reson Med 1995;33:237–245. [PubMed: 7707915]
4. Halpern HJ, Spencer DP, Polen JV, Bowman MK, Nelson AC, Dowey EM, Teicher BA. Imaging radio frequency electron spin resonance spectometer with high resolution and sensitivity for in vivo mesurements. Rev Sci Instrum 1989;60:1040–1050.
5. Kuppusamy P, Chzhan M, Vij K, Shteynbuk M, Lefer DJ, Giannella E, Zweier JL. Three-dimensional spectral-spatial EPR imaging of free radicals in the heart: a technique for imaging tissue metabolism and oxygenation. Proc Natl Acad Sci USA 1994;91:3388–3392. [PubMed: 8159757]
6. Kuppusamy P, Chzhan M, Zweier JL. Development and optimization of three-dimensional spatial EPR imaging for biological organs and tissues. J Magn Reson Ser B 1995;106:122–130. [PubMed: 7850182]
7. McCallum SJ, Nicholson I, Lurie DJ. Multimodality magnetic resonance systems for studying free radicals in vivo. Phys Med Biol 1998;43:1857–1861. [PubMed: 9703048]

8. Woods RK, Liu KJ, Walczak T, O'Hara JA, Jiang J, Swartz HM. 3-Di-mensional electron-spin resonance imaging. J Magn Reson 1989;84:247–254.
9. Halpern HJ, Peric M, Yu C, Barth ED, Chandramouli GV, Makinen MW, Rosen GM. In vivo spin-label murine pharmacodynamics using low-frequency electron paramagnetic resonance imaging. Biophys J 1996;71:403–409. [PubMed: 8804623]
10. Halpern HJ, Yu C, Peric M, Barth ED, Karczmar GS, River JN, Grdina DJ, Teicher BA. Measurement of differences in pO2 in response to perfluo-rocarbon/carbogen in FSa and NFSa murine fibrosarcomas with low-frequency electron paramagnetic resonance oximetry. Radiat Res 1996;145:610–618. [PubMed: 8619027]
11. Kuppusamy P, Chzhan M, Samouilov A, Wang P, Zweier JL. Mapping the spin-density and lineshape distribution of free radicals using 4D spectral-spatial EPR imaging. J Magn Reson Ser B 1995;107:116–125. [PubMed: 7599947]
12. Kuppusamy P, Chzhan M, Wang P, Zweier JL. Three-dimensional gated EPR imaging of the beating heart: time-resolved measurements of free radical distribution during the cardiac contractile cycle. Magn Reson Med 1996;35:323–328. [PubMed: 8699943]
13. Kuppusamy P, Shankar RA, Zweier JL. In vivo measurement of arterial and venous oxygenation in the rat using 3D spectral-spatial electron paramagnetic resonance imaging. Phys Med Biol 1998;43:1837–1844. [PubMed: 9703045]
14. Lurie DJ. Commentary: electron spin resonance imaging studies of biological systems. Br J Radiol 1996;69:983–984. [PubMed: 8958011]
15. Matsumoto K, Hyodo F, Matsumoto A, Koretsky AP, Sowers AL, Mitchell JB, Krishna MC. High-resolution mapping of tumor redox status by magnetic resonance imaging using nitroxides as redox-sensitive contrast agents. Clin Cancer Res 2006;12:2455–2462. [PubMed: 16638852]
16. Matsumoto K, Subramanian S, Devasahayam N, Aravalluvan T, Murugesan R, Cook JA, Mitchell JB, Krishna MC. Electron paramagnetic resonance imaging of tumor hypoxia: enhanced spatial and temporal resolution for in vivo pO2 determination. Magn Reson Med 2006;55:1157–1163. [PubMed: 16596636]
17. Zweier JL, Kuppusamy P. Electron paramagnetic resonance measurements of free radicals in the intact beating heart: a technique for detection and characterization of free radicals in whole biological tissues. Proc Natl Acad Sci USA 1988;85:5703–5707. [PubMed: 2840672]
18. Andrew ER. N.m.r. imaging of intact biological systems. Phil Trans R Soc Lond B Biol Sci 1980;289:471–481. [PubMed: 6106221]
19. Bates TE, Williams SR, Gadian DG, Bell JD, Small RK, Iles RA. 1H NMR study of cerebral development in the rat. NMR Biomed 1989;2:225–229. [PubMed: 2641896]
20. Eldeman RR, Warach S. Magnetic resonance imaging. N Engl J Med 1993;328:708–716. 785–791. [PubMed: 8433731]
21. Gadian, DG. NMR and its applications to living systems. Oxford Science Publications; 1995.
22. Maudsley AA, Hilal SK, Perman WH, Simon HE. Spatially resolved high resolution spectroscopy by four dimensional NMR. J Magn Reson 1983;51:147–152.
23. Lurie DJ, Davies GR, Foster MA, Hutchison JM. Field-cycled PEDRI imaging of free radicals with detection at 450 mT. Magn Reson Imaging 2005;23:175–181. [PubMed: 15833609]
24. Li H, He G, Deng Y, Kuppusamy P, Zweier JL. In vivo proton electron double resonance imaging of the distribution and clearance of nitroxide radicals in mice. Magn Reson Med 2006;55:669–675. [PubMed: 16463344]
25. He G, Deng Y, Li H, Kuppusamy P, Zweier JL. EPR/NMR co-imaging for anatomic registration of free-radical images. Magn Reson Med 2002;47:571–578. [PubMed: 11870845]
26. Matsumoto S, Nagai M, Yamada K, Hyodo F, Yasukawa K, Muraoka M, Hirata H, Ono M, Utsumi H. A composite resonator assembly suitable for EPR/NMR coregistration imaging. Concepts Magn Reson 2005;25:1–11.
27. Hutchison JM. Electron spin resonance spectrometry on the whole mouse in vivo: optimum frequency considerations. J Physics E Sci Instrum 1971;4:703–704.
28. Kuppusamy P, Zweier JL. Cardiac applications of EPR imaging. NMR Biomed 2004;17:226–239. [PubMed: 15366025]

29. Eaton, GR.; Eaton, SS.; Rihard, GA. Frequency dependence of EPR sensitivity. In: Blumler, P.; Blumich, B.; Botto, R.; Fukushima, E., editors. Spatially resolved magnetic resonance. Weinheim: Wiley-VCH; 1998.

30. Kuppusamy P, Wang P, Zweier JL. Three-dimensional spatial EPR imaging of the rat heart. Magn Reson Med 1995;34:99–105. [PubMed: 7674904]

31. He G, Shankar RA, Chzhan M, Samouilov A, Kuppusamy P, Zweier JL. Noninvasive measurement of anatomic structure and intraluminal oxygenation in the gastrointestinal tract of living mice with spatial and spectral EPR imaging. Proc Natl Acad Sci USA 1999;96:4586–4591. [PubMed: 10200306]

32. Zweier JL, Kuppusamy P. EPR spectroscopy of free radicals in the perfused heart. Curr Top Biophysics 1994;18:14–25.

33. Freed JH, Leniart DS, Hyde JS. Theory of saturation and double resonance effects in ESP spectra. RF coherence and line shapes. J Chem Phys 1967;47:2762–2773.

34. Reddy TJ, Iwama T, Halpern HJ, Rawal VH. General synthesis of persistent trityl radicals for EPR imaging of biological systems. J Org Chem 2002;67:4635–4639. [PubMed: 12098269]

35. Xia S, Villamena FA, Hadad CM, Kuppusamy P, Li Y, Zhu H, Zweier JL. Reactivity of molecular oxygen with ethoxycarbonyl derivatives of tetrathiatriarylmethyl radicals. J Organic Chem 2006;71:7268–7279.

36. He G, Evalappan SP, Hirata H, Deng Y, Petryakov S, Kuppusamy P, Zweier JL. Mapping of the B1 field distribution of a surface coil resonator using EPR imaging. Magn Reson Med 2002;48:1057–1062. [PubMed: 12465117]

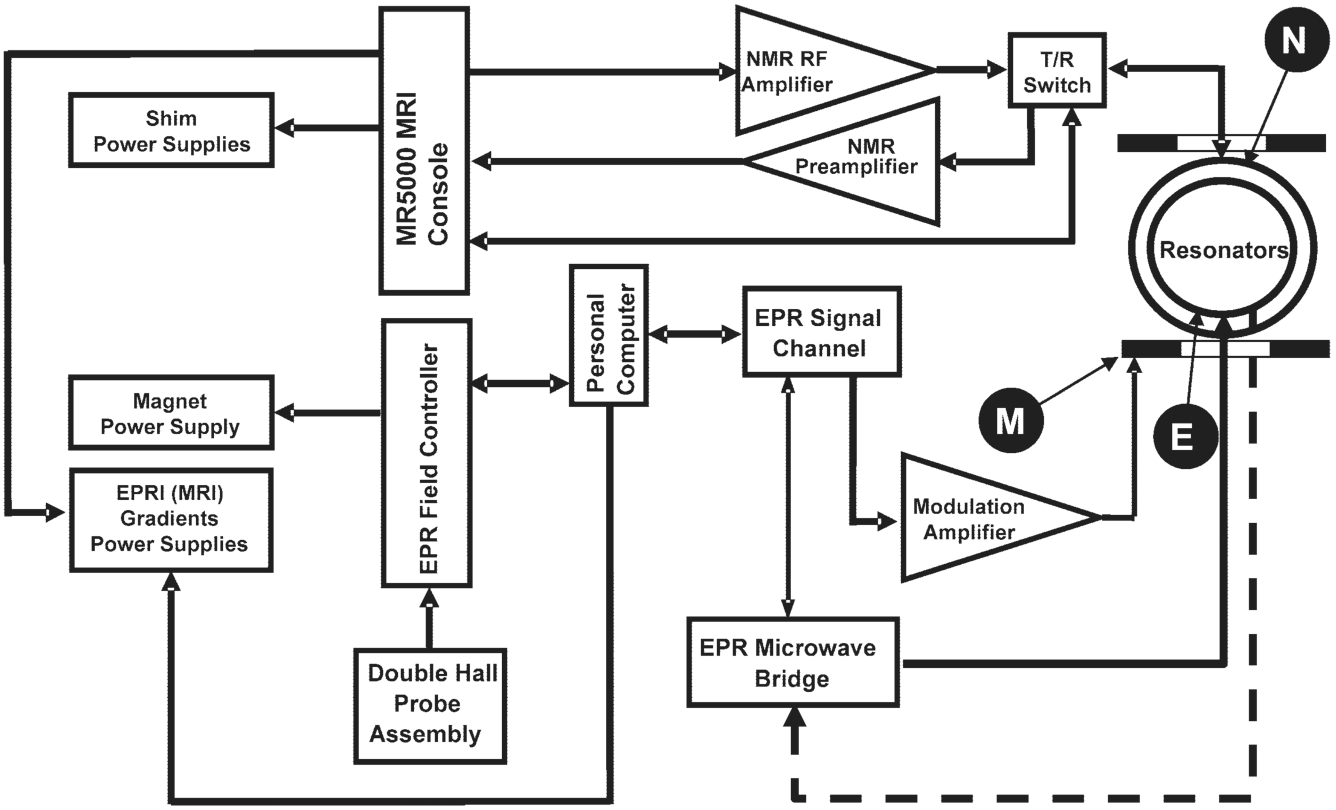

FIG. 1.
General block diagram of the coimaging system. M, modulation coils; E, EPRI resonator; N, proton NMR resonator.

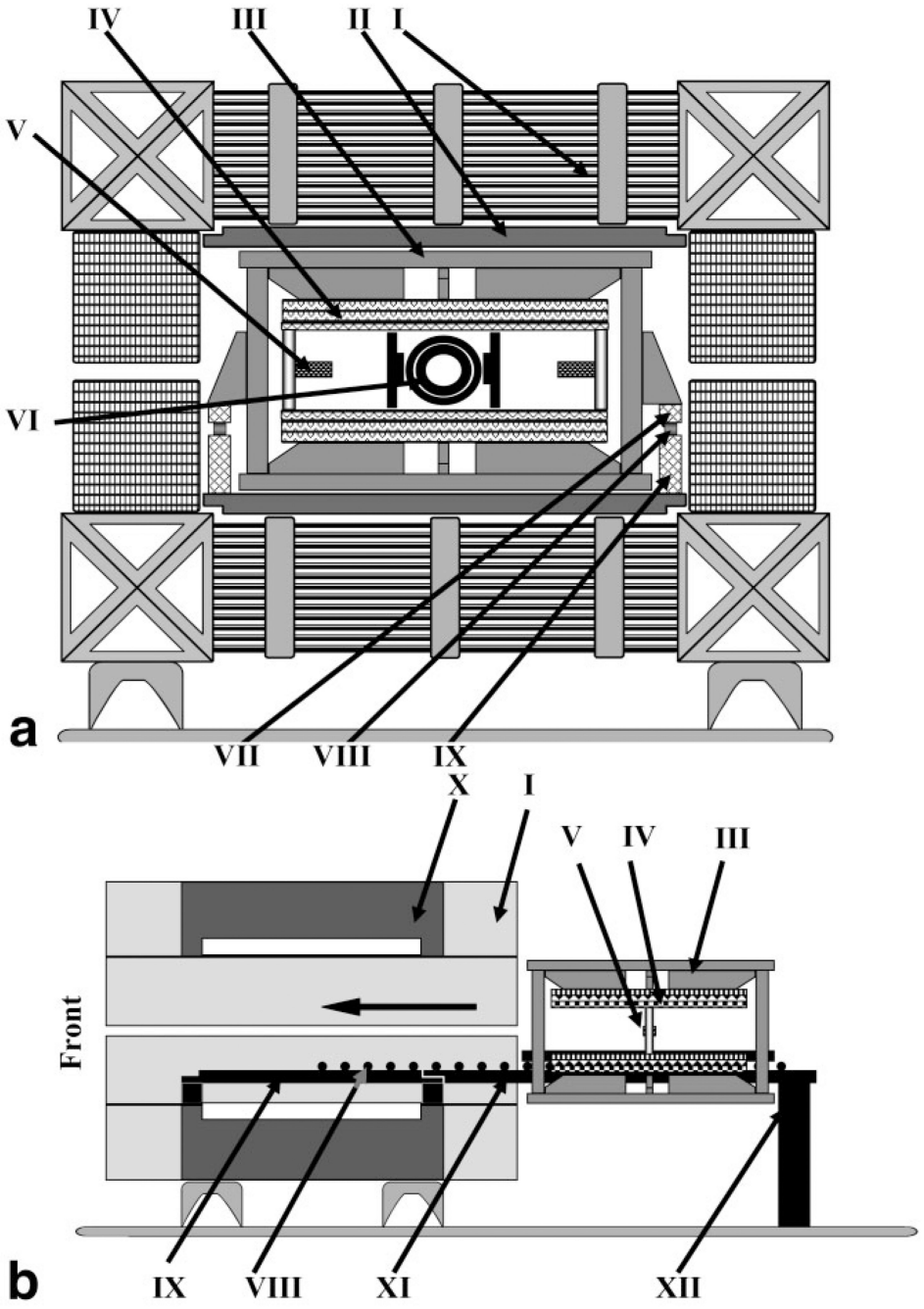

FIG. 2.

a: Schematic diagram of the mechanical layout of the co-imaging magnet system: I) main magnet coils (iron core omitted from the diagram for simplicity), II) iron shims, III) movable support frame, IV) gradient coil assembly (upper, lower without arrow), V) hall probe(s) (left, right without arrow), VI) resonators assembly, VII) upper rail, VIII) rollers, and IX) lower rail. **b:** Diagram showing the mobility of the gradient coil assembly inside the magnet. System shown without resonator assembly and with rail extension attached to the back of the magnet: I) main magnet coils, III) movable support frame, IV) gradient coil assembly (upper and lower), V) hall probe(s), VIII) linear roll bearings, IX) lower rail, X) iron core, XI) lower rail extension, and XII) rear support.

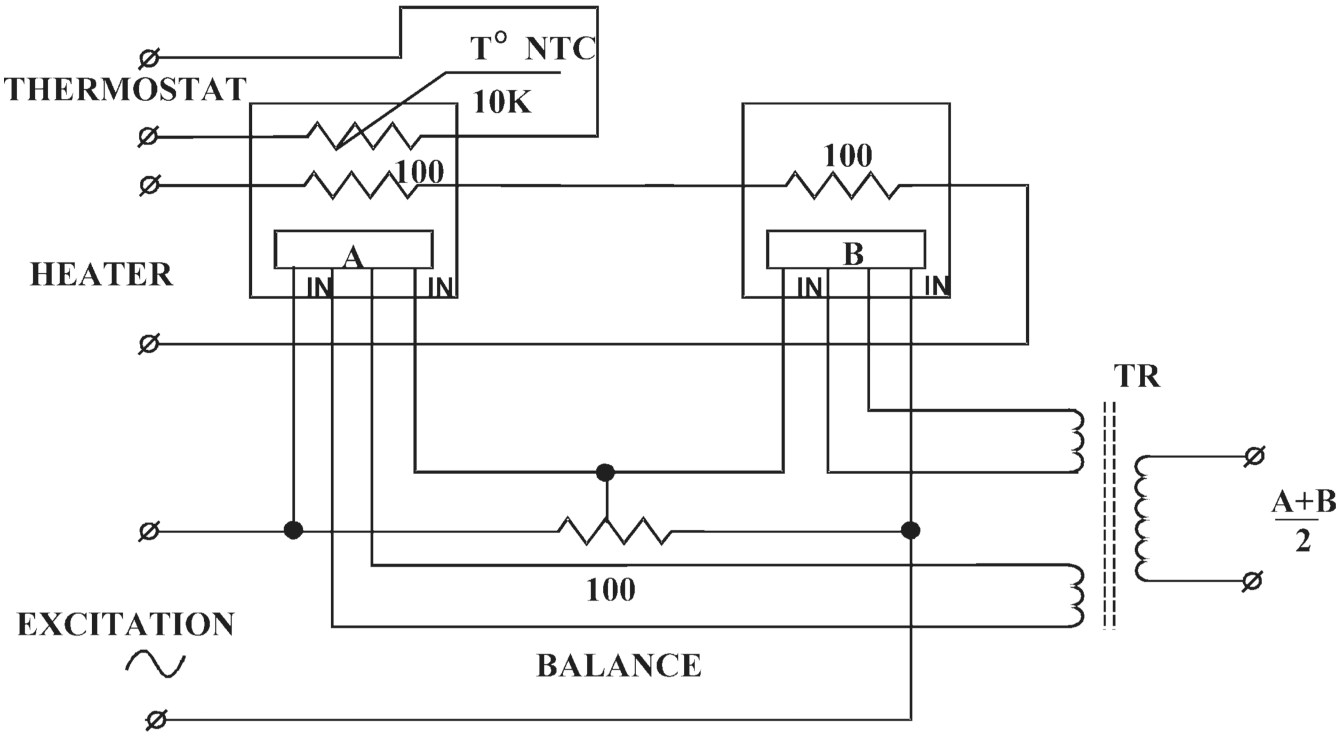

FIG. 3.
Schematic diagram of the dual-Hall-probe setup for closed-loop feedback magnetic field control that is utilized for EPRI.

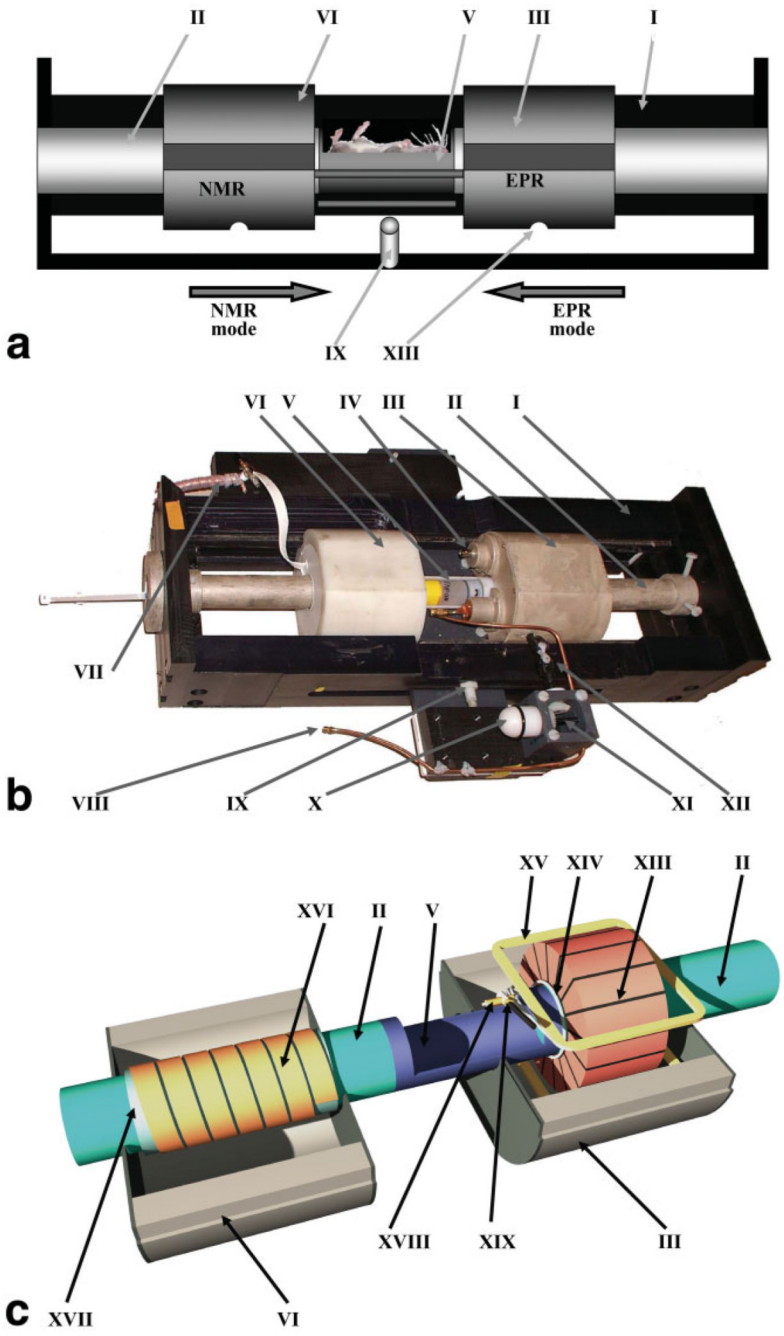

FIG. 4.

a. Diagram of the assembly with movable EPR and NMR resonators: I) body of the assembly, II) sample-holder support tube, III) EPR resonator housing, V) sample-holder, VI) NMR resonator housing, IX) spring-loaded stop plunger, and XIII) resonator positioning stop hole. **b:** Photo of the assembly with movable EPRI and proton MRI resonators: I) side walls of the assembly with tongues, II) support tube for sample-holder, III) EPR resonator (inside sliding case), IV) modulation connector, V) sample-holder (shown with sample vial in place), VI) NMR resonator (inside sliding case), VII) NMR RF connector, VIII) EPR RF connector, IX) resonator position locking mechanism (spring-loaded stop plunger), X) EPR resonator coupling adjustment knob, XI) conical gear box for coupling adjustment, and XII)

joint for resonator coupling adjustment. **c:** Diagram of the EPR and NMR resonators: II) support tube for sample-holder, III) EPR resonator housing, V) sample-holder, VI) NMR resonator housing, XIII) EPR resonator, XIV) coupling loop, XV) modulation coil (upper), XVI) NMR resonator, XVII) NMR resonator support tube, XVIII) EPR RF feeding cable, and XIX) EPR coupling capacitor.

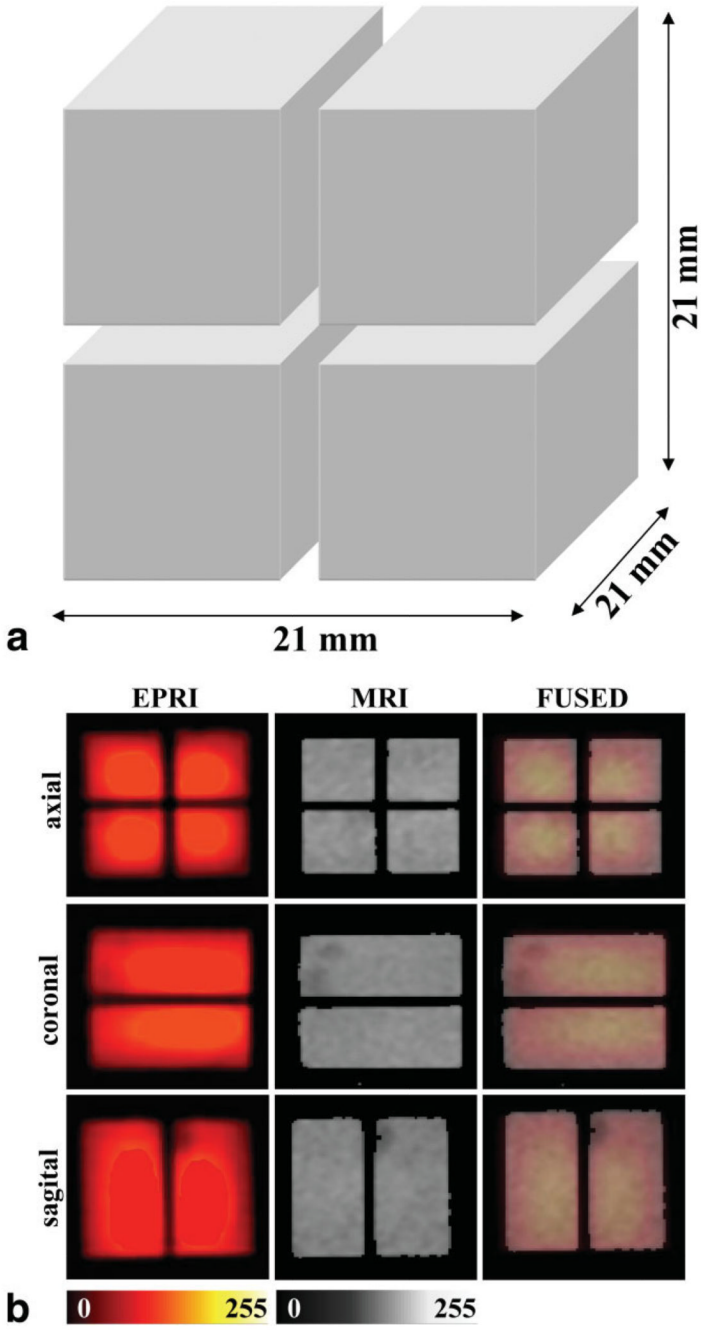

FIG. 5.

a: Diagram of the phantom used for gradient calibration. **b:** 2D images of this phantom. From left to right the images show EPR images, proton MR images, and the fused result of EPR and proton MR images. Upper row: axial view; middle row: coronal view; lower row: sagittal view. Color scale: EPRI, hot metal scale; MRI, grayscale. The EPR images set at 25% transparency were fused with the proton MRI image so that the MRI layer is visible through the EPRI layer. Images are cropped and shown with reduced FOV. MRI data were acquired with a receiver bandwidth of 10 kHz using a 2D gradient-echo (GRE) sequence (matrix = 128 × 128, FOV = 40 × 40 mm, TR = 750 ms, TE = 39 ms, number of excitations (NEX) = 4, slice thickness = 21 mm, set to span over the whole object thickness). The

parameters used for the EPRI acquisition were as follows: frequency = 1.19 GHz, microwave power = ~300 mW, modulation amplitude = 0.07 mT, field gradient = 0.5 mT/cm, scan time = 3.9 s, scan width = 2 mT, and 32 projections for each 2D acquisition. The measured SNRs on separate slices of EPR and NMR images gave values of 25.3 and 6.6, respectively. SNR was calculated as the ratio of intensities from the image to the background. Each area was averaged. Values were taken from 128 × 128 matrices before bilinear interpolation.

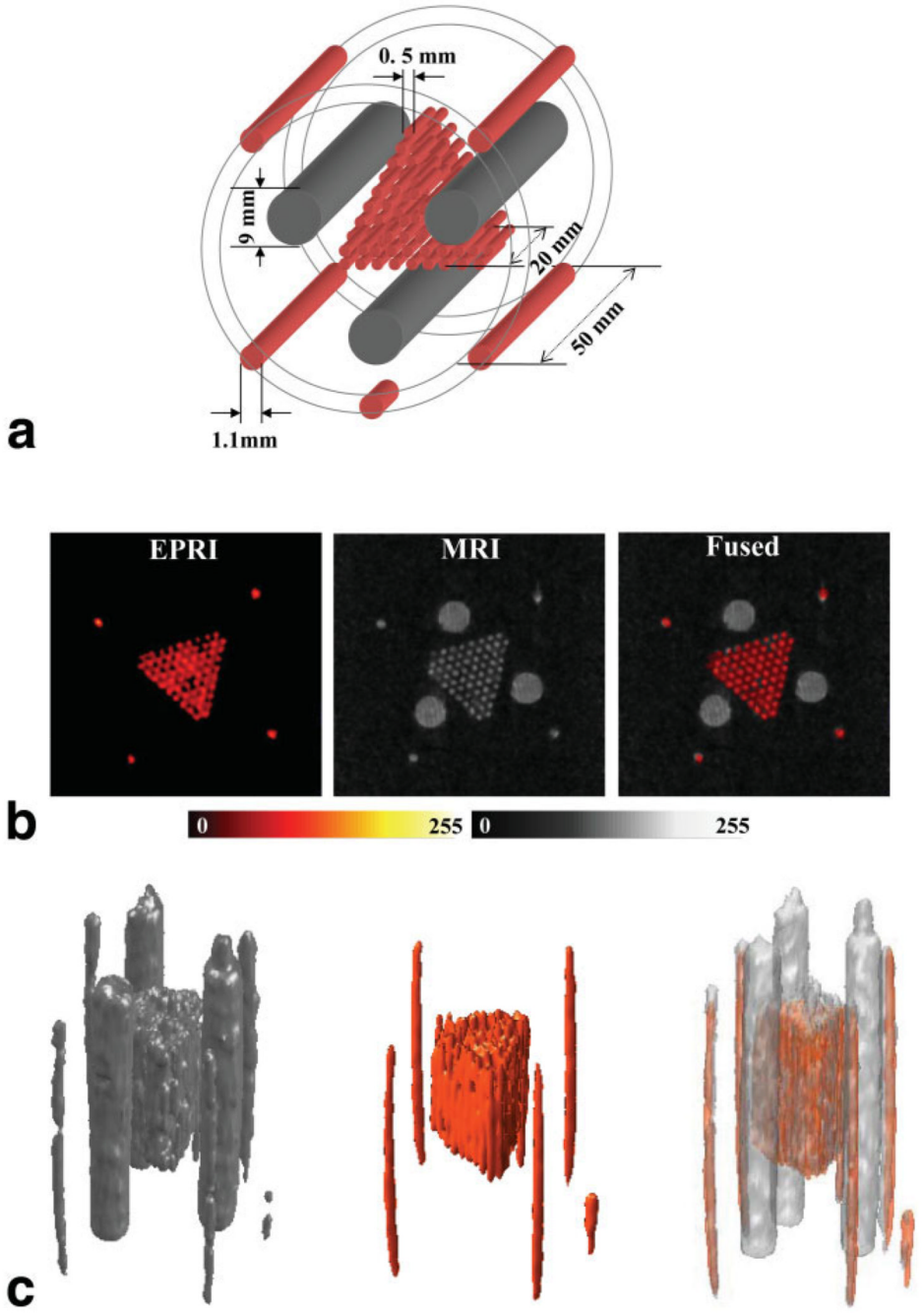

FIG. 6.

a: Diagram of the phantom used for the instrument resolution assessment. **b:** Set of axial slices of the sample shown in part **a**, showing from left to right the EPR image, the proton MR image, and the fused coimage. Color scale: EPRI, hot metal scale; MRI, grayscale. **c:** Views of the 3D rendering of the full data from MRI (grayscale) and EPRI (color scale). The right-most figure shows the fused result. The rendered surfaces of the 3D data are shown with a transparency of 60%. The MRI dataset was acquired using a GRE pulse sequence with the following parameters: matrix = 128 × 128 × 128, TR = 47 ms, TE = 20 ms, NEX = 1, FOV in plane = 40 × 40 mm, FOV in slice direction = 100 mm (transversal slice thickness = 0.78 mm), flip angle = 65°. The parameters used for the EPRI acquisition were as follows:

frequency = 1.19 GHz, microwave power = ~300 mW, modulation amplitude = 0.025 mT at 100 kHz, field gradient = 0.5 mT/cm along the X and Z directions and 0.2 mT/cm along Y, scan time = 2.6 s, 32 × 32 projections, and scan width = 2 mT. The measured SNRs on separate slices of EPR and NMR images gave values of 14.6 and 6.9, respectively.

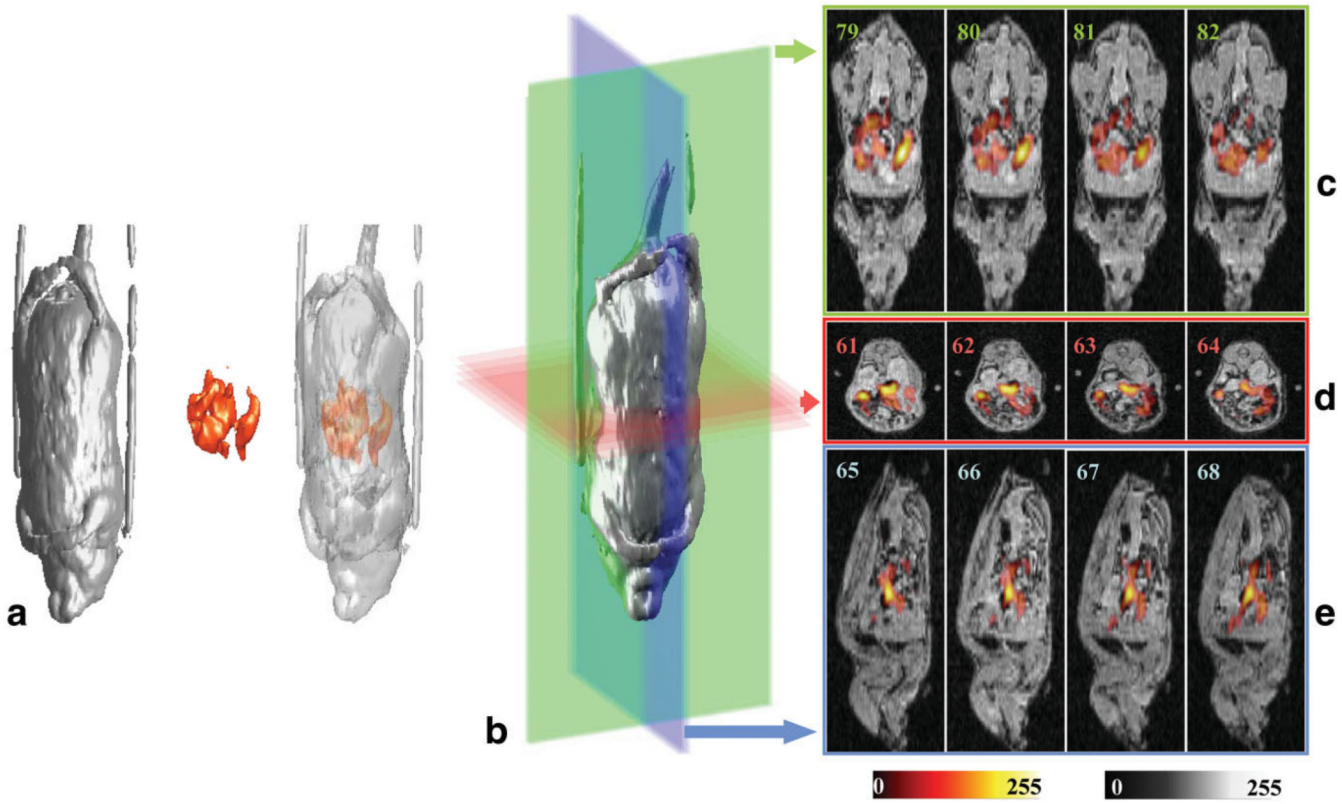

FIG. 7.

a: 3D renderings of the proton MRI, EPRI, and fused images from a live mouse fed paramagnetic charcoal. **b:** 3D rendering of the MR image dataset showing the planes for the slices depicted in **c–e**. Colors of the planes correspond to the frames containing the slices shown: (**c**) coronal slices, (**d**) axial slices, and (**e**) sagittal slices of the fused images. Color scale: MRI, grayscale; EPRI, hot metal scale. The MRI data were acquired using a GRE pulse sequence with the following parameters: bandwidth = 12.5 kHz, matrix = 128 × 128 × 128, TR = 70 ms, TE = 10 ms, NEX = 1, FOV in plane = 50 × 50 mm, FOV in slice direction = 130 mm (transverse slice thickness = 1.01 mm), and flip angle = 65°. The total acquisition time was 19 min. The parameters used for the EPRI acquisition were as follows: frequency = 1.19 GHz, microwave power = 300 mW, modulation amplitude = 0.05 mT, scan width = 4 mT, maximum field gradient = 0.8 mT/cm along the X and Z directions and 0.307 mT/cm along Y, projection number = 256, scan time = 1.3 s, total acquisition time = 6 min. Measured SNRs on separate slices of EPR and NMR images gave values of 13.8 and 10.5, respectively.